

Giant Reversible Piezoelectricity from Symmetry-Governed Stochastic Dipole Hopping

Denan Li,^{1,2} Haofei Ni,³ Yi Zhang,³ and Shi Liu^{2,4,*}

¹*Fudan University, Shanghai 200433, China*

²*Department of Physics, School of Science,*

Westlake University, Hangzhou, Zhejiang 310030, China

³*Institute for Science and Applications of Molecular Ferroelectrics,*

Key Laboratory of the Ministry of Education for Advanced Catalysis Materials,

Zhejiang Normal University, Jinhua, Zhejiang 321004, China

⁴*Institute of Natural Sciences, Westlake Institute for Advanced Study,*

Hangzhou, Zhejiang 310024, China

Abstract

Organic–inorganic hybrid perovskites with giant piezoelectric responses, exemplified by TMCM-CdCl₃, represent a promising platform for flexible and environmentally friendly electromechanical materials. However, the microscopic origin of such exceptional performance in this weakly polar system has remained elusive. Here, using deep-learning-assisted large-scale molecular dynamics simulations, we resolve this paradox by reproducing the experimentally measured piezoelectric coefficient $d_{33} \approx 220$ pC/N, and demonstrating that the giant response arises from the collective contribution of multiple intrinsic components, particularly the shear component d_{15} . This effect does not stem from conventional polarization rotation or phase switching, but instead originates from stochastic 120° in-plane rotational hopping of a small fraction of organic cations. This discrete hopping mechanism is governed by the local C₃-symmetric halogen-bonding network between the host framework and the guest cation. The Arrhenius-type temperature dependence of d_{15} further confirms the role of thermally activated dipole hopping. This work provides a clear pathway to enhance piezoelectric performance of hybrid materials through rational engineering of host–guest interactions.

* liushi@westlake.edu.cn

Piezoelectric materials, which can convert mechanical energy into electrical energy and vice versa, are foundational to a wide range of modern technologies, from ultrasound to advanced sensors [1]. For decades, this technological landscape has been dominated by inorganic ferroelectrics such as barium titanate (BTO) and lead zirconate titanate (PZT) [2–6]. While these materials offer robust performance, they also present notable drawbacks: they are heavy, brittle, require high-temperature processing, and often contain toxic elements, making them unsuitable for emerging applications that demand flexible, lightweight, and biocompatible piezoelectrics. This has driven a search for molecular alternatives, which promise mechanical flexibility and environmentally friendly solution-processability, but have historically been limited by a fundamental trade-off: molecular ferroelectrics tend to exhibit low spontaneous polarization, leading to weak piezoelectric response [7–11].

The discovery of the hybrid organic-inorganic ferroelectric perovskite trimethylchloromethyl ammonium trichlorocadmium(II) $[\text{Me}_3\text{NCH}_2\text{ClCdCl}_3]$, (TMCM- CdCl_3), composed of organic TMCM^+ cations and inorganic CdCl_3^- frameworks, marks an important advancement [12]. Exhibiting a giant piezoelectric coefficient, it challenges the long-standing trade-off typically associated with molecular ferroelectrics. This breakthrough opens up new opportunities for developing flexible, low-temperature-processable piezoelectric materials. However, it also presents a fundamental paradox: despite having a spontaneous polarization of only $4\text{--}5\text{ }\mu\text{C}/\text{cm}^2$, an order of magnitude smaller than that of BTO ($\approx 25\mu\text{C}/\text{cm}^2$), TMCM- CdCl_3 achieves a piezoelectric strain coefficient of $d_{33} \approx 220\text{ pC/N}$, comparable to BTO. The striking anomaly of a weakly polar material exhibiting a giant piezoelectric response suggests the presence of an unconventional physical mechanism.

Two primary theories have been proposed to resolve the paradox of giant piezoelectricity in weakly polar TMCM-based perovskites. The original study suggested a ferroelastic polarization rotation mechanism [12]. Crystallographic and vector piezoresponse force microscopy analyses revealed that monoclinic TMCM- CdCl_3 hosts twelve energetically equivalent polar states. It was argued that applied stress could trigger ferroelastic switching between these states, causing a large-angle reorientation of the polarization vector and, consequently, a giant piezoelectric response. A key limitation of this theory is that reversible ferroelastic switching, essential for reversible piezoelectricity, often requires alternating compressive and tensile stress, a condition not typically met during standard unipolar piezoelectric measurements. A later theoretical study proposed a phase-switching mechanism [13]. First-principles

calculations identified a metastable phase featuring TMCM⁺ cations in head-to-head and tail-to-tail orientations. The piezoelectric response was attributed to a stress-induced transition between this phase and the ground-state monoclinic structure. This theory was based on static, zero-Kelvin unit-cell calculations that neglect thermal fluctuations and collective dipole dynamics, factors likely crucial to understanding the experimental behavior at finite temperatures and in mesoscale systems.

Here, we resolve this long-standing puzzle using large-scale molecular dynamics (MD) simulations of TMCM-CdCl₃, enabled by a high-fidelity machine-learning force field trained exclusively on first-principles data. By computing the full piezoelectric tensor in the single-domain limit at 300 K, we show that the experimentally observed giant response is dominated not by the intrinsic longitudinal coefficient d_{33} , but by large shear components, particularly $d_{15} = 163$ pC/N. Notably, applying a proper tensor transformation from the crystal to the laboratory frame yields an effective d_{33}^{eff} of 212 pC/N at 300 K, closely matching the experimental value of 220 pC/N. We uncover a novel piezoelectric mechanism distinct from both ferroelastic and phase switching: a stress-driven, thermally-activated stochastic 120° rotational hopping of a small fraction of TMCM⁺ cations. This hopping is governed by the local C₃ symmetry imposed by the halogen bonds between organic cations and the inorganic framework. As long as the fraction of hopped cations remains below a critical threshold, they can return to their original states once the stress is removed, exhibiting a shape-memory-like effect. This collective, reversible dipole hopping underlies the observed reversible piezoelectricity, further supported by the strong temperature dependence of the response. Finally, we distinguish this useful, reversible behavior from the irreversible, large-strain ferroelastic switching that defines the material’s fatigue limit. Our results provide a comprehensive picture of piezoelectricity in TMCM-CdCl₃ and similar hybrid perovskites, offering key insights for further improving electromechanical responses in these materials.

Previous studies have shown that TMCM-CdCl₃ crystallizes in the monoclinic space group *Cc* in the ferroelectric phase and the hexagonal space group *P6₃/mmc* in the paraelectric phase. Despite several DFT-based investigations, the connection between the collective orientations of molecular dipoles associated with TMCM⁺ cations and the macroscopic polarization remains controversial in literature [13–15]. We introduce an intuitive host-guest framework to clarify this relationship. As depicted in Fig. 1a, one-dimensional CdCl₃[−] chains, the “host,” self-assemble into a triangular lattice, forming triangular channels along the

[001] direction. The functional “guests” are organic TMCM^+ cations, which reside within these channels and form their own A-B stacked triangular sub-lattices. In the paraelectric phase, the molecular cations are fully disordered, yielding a primitive hexagonal unit cell. In contrast, the ferroelectric phase features alignment of the out-of-plane components of all molecular dipoles (Fig. 1b). However, a previously underappreciated detail is that, while dipoles within each layer are aligned, adjacent layers of dipoles are not fully co-aligned, as seen in the side view (Fig. 1b) and top-down view (Fig. 1c). We find that the orientation of each TMCM^+ cation is anchored by highly directional $\text{CH}_3\text{-Cl}\cdots\text{Cl}$ halogen bonds (see dashed lines in Fig. 1b-c), which act as a “molecular lock” connecting the guest cation to the surrounding inorganic chains. This interaction restricts the cation to one of three energetically equivalent orientations, with its intrinsic (in-plane) dipole pointing toward an edge of the triangular channel. The helical arrangement of Cl atoms along the CdCl_3^- chains therefore prevents full dipole alignment across layers.

Since the unit cell of the ferroelectric phase contains two layers of molecular dipoles, the in-plane component of the total polarization can be intuitively understood using the schematic in Fig. 1f, which represents each dipole layer as a triangle, with the two triangles rotated 180° relative to each other to reflect the stacking arrangement. The six macroscopic polar variants along the [102] and other crystallographically equivalent directions, illustrated in Fig. 1d, correspond to distinct combinations of allowed relative orientations between the two layers of TMCM^+ cations within the unit cell. As discussed in detail below, the restricted molecular dipole orientations, governed by the C_3 symmetry, play a key role in the piezoelectric response.

Theoretical prediction of finite-temperature piezoelectric coefficients in hybrid materials such as TMCM-CdCl_3 is challenging, as conventional approaches such as density functional perturbation theory often yield negligible values [13, 16]. This limitation likely arises from the neglect of thermal fluctuations and the associated order-disorder behavior of molecular dipoles. To overcome this challenge, we developed a deep neural network-based interatomic potential (deep potential, or DP [17, 18]), which enables large-scale MD simulations of TMCM-CdCl_3 at finite temperatures. It can also directly predict total polarization from atomic positions. Our model demonstrates high fidelity across a wide range of validation tests. It achieves an excellent fit to the reference DFT database, with low mean absolute errors (MAEs) for energy (0.214 meV/atom), force (0.017 eV/Å), virial (1.609 meV/atom),

and polarization ($0.06 \mu\text{C}/\text{cm}^2$). The model accurately reproduces static properties, including the equation of state and elastic moduli, and captures key dynamic and finite-temperature phenomena, such as the energy barrier for in-plane TMCM⁺ cation rotation and the temperature-driven ferroelectric-to-paraelectric phase transition (see Supplementary Material for details, [19–31]). The piezoelectric tensor element is calculated as $d_{ij} = \Delta P_i / \sigma_j$, reflecting the polarization change along direction i (ΔP_i) due to an applied stress with component j (σ_j in Voigt notation).

We now explain the calculation of d_{15} (with indices defined relative to the monoclinic unit cell) in detail. A shear deformation is imposed by varying the lattice angle β by an amount $\Delta\beta$ (Fig. 2a inset), while allowing all other lattice parameters to fully relax during finite-temperature MD simulations with β held fixed, using a 10,800-atom supercell. At equilibrium, only the shear stress component σ_5 is nonzero, establishing a one-to-one relationship among $\Delta\beta$, σ_5 , and P_1 . The evolution of P_1 and σ_5 as a function of $\Delta\beta$ at 300 K is shown in Fig. 2, along with dipole density plots that illustrate the distributions of in-plane molecular dipole orientations within the supercell. The starting polar state I has a net in-plane polarization along the $[\bar{1}00]$ direction ($P_1 \approx -4 \mu\text{C}/\text{cm}^2$). As shear strain is applied, the shear stress σ_5 increases in magnitude, while all other stress components (σ_j , $j \neq 5$) remain negligible (Fig. 2b). This confirms that in MD simulations, the system reaches mechanical equilibrium under the constraint of fixed $\Delta\beta$, with σ_5 representing the balanced internal stress required to maintain the imposed deformation. The microstructural evolution under shear is revealed by the dipole density plots (Fig. 2f). In the strained state II, MD simulations show that dipoles do not rotate uniformly. Instead, a subset of molecular dipoles undergo 120° hops into adjacent symmetry-equivalent potential wells. These locally reoriented dipoles act as “orientational defects” embedded within the original domain [15].

Notably, the shear stress σ_5 reaches its maximum value, σ_5^t , at a critical shear deformation $\Delta\beta^t \approx 2.8^\circ$, marking the threshold for piezoelectric reversibility. State II lies just below this threshold. When the stress is removed, the system relaxes to state II' (see Fig. 2f), which is nearly identical to the initial state I. This indicates that dipoles return to their original orientations via reverse 120° hopping, resulting in a fully reversible piezoelectric response. In contrast, when the applied shear strain exceeds the threshold ($\Delta\beta > \Delta\beta^t$), the system transitions to a fundamentally different configuration, represented by state III, characterized by a more isotropic distribution of in-plane dipole orientations. After unloading, the system

relaxes to state III', where dipoles occupy four symmetry-related wells, clearly distinct from the initial state I. These results demonstrate that the critical stress σ_5^t associated with $\Delta\beta^t$ defines the limit for reversible piezoelectric switching. We thus define the reversible shear piezoelectric coefficient as $d_{15} = \Delta P_1^t / \sigma_5^t = 163$ pC/N.

TABLE I. Intrinsic piezoelectric strain tensor (in pC/N) calculated from MD simulations in the crystal frame, and the effective piezoelectric strain tensor (d^{eff}) in the laboratory frame, both presented in matrix form. The largest component is highlighted in bold.

d_{ij}	Crystal Frame (intrinsic)	Laboratory Frame (d^{eff})
$\begin{pmatrix} d_{11} & d_{12} & d_{13} & d_{14} & d_{15} & d_{16} \\ d_{21} & d_{22} & d_{23} & d_{24} & d_{25} & d_{26} \\ d_{31} & d_{32} & d_{33} & d_{34} & d_{35} & d_{36} \end{pmatrix}$	$\begin{pmatrix} 77 & 54 & 27 & -1 & \mathbf{163} & 40 \\ -15 & -37 & -14 & 32 & 16 & -135 \\ 25 & 11 & 14 & 0 & 45 & 0 \end{pmatrix}$	$\begin{pmatrix} -47 & 23 & 78 & 15.6 & -7 & 13 \\ -30 & -37 & 0 & -89 & -5 & -105 \\ -104 & 11 & \mathbf{211} & 28 & -22 & 22 \end{pmatrix}$

Table I presents the intrinsic piezoelectric tensor, calculated in the single-crystal, single-domain limit at 300 K using the method described above. Interestingly, the longitudinal component d_{33} is relatively low at 14 pC/N, while the components $d_{15} = 163$ pC/N and $d_{11} = 77$ pC/N are significantly larger in magnitude. This indicates that stress applied along the crystallographic c -axis induces minimal polarization change, reflecting the structural rigidity of the CdCl_3^- inorganic chains.

Experimentally, as-grown ferroelectric monoclinic TMCM- CdCl_3 thin films typically adopt the (110) orientation [or the equivalent (100) orientation in the paraelectric phase] [32]. As a result, the stress applied along the film normal direction, denoted σ^Z (aligned with the laboratory Z -axis), does not coincide with the crystallographic c -axis. Consequently, the effective piezoelectric coefficient measured along Z , d_{33}^{eff} , reflects a combination of multiple components of the intrinsic piezoelectric tensor. To quantitatively connect the intrinsic response to the experimental geometry, we perform a tensor rotation to identify the relative orientation between the stress along the film normal and polarization direction that maximizes d_{33}^{eff} . We find that d_{33}^{eff} reaches a value of 211 pC/N when σ^Z is nearly orthogonal to $[0\bar{1}2]$ or $[01\bar{2}]$ polarization vectors (see schematic in Fig. S7), in excellent agreement with the experimentally measured value of 220 pC/N.

The origin of the enhanced effective response, exceeding that of any single intrinsic component, can be understood as follows. Due to the relative freedom of molecular cations in

the host-guest framework of TMCM-CdCl₃. The polarization vector does not align with any of the unit cell's crystallographic axes in the ferroelectric monoclinic phase. This anisotropy allows σ^Z to project onto multiple stress components in the crystal frame: $\sigma^Z = 0.5\sigma_1 + 0.4\sigma_3 + 0.5\sigma_5$. As a result, the effective response includes weighted contributions from several intrinsic tensor elements, specifically d_{11} , d_{13} , d_{15} , d_{31} , d_{33} , and d_{35} , which collectively yield the giant piezoelectric response of 211 pC/N. We find that d_{15} and d_{11} account for about 60% and 20% of d_{33}^{eff} , respectively.

The excellent agreement between theory and experiment not only validates our finite-temperature MD-based approach for computing the intrinsic piezoelectric tensor, but also provides microscopic insights into the origin of the giant response. Microscopically, the giant piezoelectric response of TMCM-CdCl₃ primarily arises from stress-driven, symmetry-governed stochastic hopping of molecular dipoles by 120°. Crucially, only a small subset of local dipoles are activated, ensuring a reversible mechanical response. This gives rise to a macroscopically small-angle rotation of the net polarization vector. As shown in Fig. 2e, $\Delta\beta^t$ corresponds to a maximum rotation of global polarization by approximately 14°, significantly smaller than previously proposed values (56°) [13], setting this mechanism apart from the conventional polarization rotation mechanism [33]. Importantly, this behavior occurs without any phase transition, in contrast to earlier interpretations [12, 13].

Since the piezoelectric response of TMCM-CdCl₃ is governed by the stochastic hopping of molecular dipoles, a process inherently influenced by thermal fluctuations, we expect the piezoelectric coefficients to exhibit strong temperature dependence. To investigate this, we construct σ_5 - $\Delta\beta$ curves at various temperatures ranging from 200 K to 350 K (Fig. 3a). From these, we derive the corresponding ΔP_1 - σ_5 curves (Fig. 3b). At each temperature, the shear piezoelectric coefficient d_{15} is estimated using the relation $d_{15} = \Delta P_1^t / \sigma_5^t$. As expected, d_{15} shows a pronounced temperature dependence, increasing from 6 pC/N at 200 K to a giant value of 823 pC/N at 350 K. We find that this temperature dependence follows an Arrhenius-type relationship: plotting $\ln d_{15}$ against $1/T$ yields a clear linear trend. The slope of this line corresponds to an activation energy (E_a) of 0.18 eV, which agrees well with the 0.21 eV rotational barrier for TMCM⁺ cations obtained from DFT calculations (see Fig. S3). The Arrhenius-type temperature dependence of the piezoelectric response demonstrates that the giant effect in TMCM-CdCl₃ at room temperatures arises from a dynamic process governed by thermally activated hopping of molecular dipoles over an energy barrier.

As discussed above, a large applied stress can induce an irreversible structural transformation when the shear distortion exceeds $\Delta\beta^t$. The turnover in the stress-strain curve beyond $\Delta\beta^t$ reflects a stress-relaxation process (Fig. 2a), conceptually analogous to plastic deformation in metals. MD simulations reveal that this relaxation occurs through the hopping of molecular dipoles, leading to the formation of “orientational defects,” which play a similar role to dislocation defects in metals that enable plasticity [34]. This analogy motivates further exploration of the mechanical response of TMCM-CdCl₃ under large shear stress or strain, which could define the material’s operational limit.

Figure 4a presents the full stress-strain curve, corresponding to an in-plane 180° ferroelastic switching event, as the monoclinic angle β is swept from 94.3° to 85.7°. During this transition, the stress passes through a local minimum at $\beta \approx 90^\circ$, which corresponds to an intermediate state characterized by a nearly in-plane isotropic distribution of molecular dipole orientations. Once the switching is complete, the molecular dipoles have exhausted all available hopping pathways. Consequently, further applied strain can only be accommodated by elastic lattice distortion, causing the stress to rise sharply and linearly, a regime we refer to as the “elastic region.” In the corresponding P_1 – σ_5 curve shown in Fig. 4b, we can define another critical stress, σ_5^* , which is the *minimum* stress required to complete the ferroelastic switching process. Assuming a quasi-equilibrium process driven by σ_5^* , the system eventually equilibrates in the elastic region when the internal stress balances σ_5^* . This allows us to define an effective piezoelectric coefficient associated with ferroelastic switching: $d_{15}^* = \Delta P_1^* / \sigma_5^* = 793$ pC/N.

However, we note that this ultrahigh response is a one-time effect under a unipolar stress condition. After unloading, the system relaxes to the $+P_1^s$ state (Fig. 4 inset). Subsequent stress application in the same direction will only operate within the elastic regime, yielding a negligible piezoelectric response. This irreversible ferroelastic switching thus acts as a fatigue mechanism, explaining how a sample could be rendered piezoelectrically inactive if driven beyond its reversible, intrinsic limit. That said, if ferroelastic switching could be harnessed in a reversible fashion, for example, through domain wall engineering, then the piezoelectric response of TMCM-CdCl₃ could potentially be enhanced by over 350%.

In summary, using finite-temperature, large-scale molecular dynamics simulations enabled by first-principles-based machine-learning force field, we have developed a robust approach to compute the full piezoelectric tensor for organic-inorganic hybrid perovskites

represented by TMCM-CdCl₃. This method captures key anharmonic effects associated with the thermally driven order–disorder behavior of molecular dipoles. We reproduce experimental giant piezoelectric coefficient, demonstrating that the effect is dominated by intrinsic components like d_{15} and d_{11} , which arise from stochastic in-plane hopping of molecular dipoles. This hopping is not random: the local C₃-symmetric halogen-bonding network between TMCM⁺ cations and the inorganic host framework creates a rotational potential energy landscape with three symmetry-equivalent minima. The Arrhenius-type temperature dependence of the piezoelectric coefficients further corroborates the critical role of dipole hopping. The mechanism of discrete, localized hopping is fundamentally different from the continuous, bulk polarization rotation that drives the response in conventional piezoceramics like PZT near a morphotropic phase boundary [33, 35]. Importantly, the reversibility of the piezoelectric response in TMCM-CdCl₃ also relies on the activation of only a small subset of molecular dipoles. We also identify in-plane 180° ferroelastic switching as both a potential fatigue mechanism and a promising route to further enhance the electromechanical response if rendered reversible. Our work underscores the potential of engineering host–guest halogen bonds to precisely tailor the rotational energy landscape of molecular dipoles for improved performance.

ACKNOWLEDGMENTS

We acknowledge the supports from National Natural Science Foundation of China (92370104). The computational resource is provided by Westlake HPC Center.

-
- [1] F. Li, B. Wang, X. Gao, D. Damjanovic, L.-Q. Chen, and S. Zhang, Ferroelectric materials toward next-generation electromechanical technologies, *Science* **389**, eadn4926 (2025).
 - [2] M. Acosta, N. Novak, V. Rojas, S. Patel, R. Vaish, J. Koruza, J. Rossetti, G. A., and J. Rödel, BaTiO₃-based piezoelectrics: Fundamentals, current status, and perspectives, *Appl. Phys. Rev.* **4**, 041305 (2017).
 - [3] M. Höfling, X. Zhou, L. M. Riemer, E. Bruder, B. Liu, L. Zhou, P. B. Groszewicz, F. Zhuo,

- B.-X. Xu, K. Durst, X. Tan, D. Damjanovic, J. Koruza, and J. Rödel, Control of polarization in bulk ferroelectrics by mechanical dislocation imprint, *Science* **372**, 961 (2021).
- [4] B. Jaffe, R. Roth, and S. Marzullo, Piezoelectric properties of lead zirconate-lead titanate solid-solution ceramics, *J. Appl. Phys.* **25**, 809 (1954).
- [5] S. Zhang, F. Li, X. Jiang, J. Kim, J. Luo, and X. Geng, Advantages and challenges of relaxor-PbTiO₃ ferroelectric crystals for electroacoustic transducers – a review, *Prog. Mater. Sci.* **68**, 1 (2015).
- [6] J. Li, W. Qu, J. Daniels, H. Wu, L. Liu, J. Wu, M. Wang, S. Checchia, S. Yang, H. Lei, R. Lv, Y. Zhang, D. Wang, X. Li, X. Ding, J. Sun, Z. Xu, Y. Chang, S. Zhang, and F. Li, Lead zirconate titanate ceramics with aligned crystallite grains, *Science* **380**, 87 (2023).
- [7] A. J. Lovinger, Ferroelectric polymers, *Science* **220**, 1115 (1983).
- [8] Y. Liu and Q. Wang, Ferroelectric polymers exhibiting negative longitudinal piezoelectric coefficient: Progress and prospects, *Adv. Sci.* **7**, 1902468 (2020).
- [9] Z. Sun, A. Zeb, S. Liu, C. Ji, T. Khan, L. Li, M. Hong, and J. Luo, Exploring a lead-free semiconducting hybrid ferroelectric with a zero-dimensional perovskite-like structure, *Angew. Chem. Int. Ed.* **55**, 11854 (2016).
- [10] H.-Y. Ye, Y.-Y. Tang, P.-F. Li, W.-Q. Liao, J.-X. Gao, X.-N. Hua, H. Cai, P.-P. Shi, Y.-M. You, and R.-G. Xiong, Metal-free three-dimensional perovskite ferroelectrics, *Science* **361**, 151 (2018).
- [11] W.-Q. Liao, D. Zhao, Y.-Y. Tang, Y. Zhang, P.-F. Li, P.-P. Shi, X.-G. Chen, Y.-M. You, and R.-G. Xiong, A molecular perovskite solid solution with piezoelectricity stronger than lead zirconate titanate, *Science* **363**, 1206 (2019).
- [12] Y.-M. You, W.-Q. Liao, D. Zhao, H.-Y. Ye, Y. Zhang, Q. Zhou, X. Niu, J. Wang, P.-F. Li, D.-W. Fu, Z. Wang, S. Gao, K. Yang, J.-M. Liu, J. Li, Y. Yan, and R.-G. Xiong, An organic-inorganic perovskite ferroelectric with large piezoelectric response, *Science* **357**, 306 (2017).
- [13] P. Ghosh, S. Lisenkov, and I. Ponomareva, Phase switching as the origin of large piezoelectric response in organic-inorganic perovskites: A first-principles study, *Phys. Rev. Lett.* **125**, 207601 (2020).
- [14] Y. Lin, C. Chai, Z. Liu, J. Wang, S. Jin, Y. Yang, Y. Gao, M. Hao, X. Li, Y. Hou, X. Ma, B. Wang, Z. Wang, Y. Kan, J. Zheng, Y. Bai, Y. Chen, J. Sun, T. Zhao, J. Y. Law, V. Franco,

- F. Hu, and B. Shen, Large low-field-driven electrocaloric effect in organic-inorganic hybrid tmcm-cdcl₃, *Nat. Commun.* **16**, 4009 (2025).
- [15] K. Tolborg and A. Walsh, Models of orientational disorder in hybrid organic–inorganic piezoelectric materials, *J. Mater. Chem. C* **11**, 8885 (2023).
- [16] E. D. Sødahl, J. Walker, and K. Berland, Piezoelectric response of plastic ionic molecular crystals: role of molecular rotation, *Cryst. Growth Des.* **23**, 729 (2023).
- [17] L. Zhang, J. Han, H. Wang, R. Car, and W. E, Deep potential molecular dynamics: A scalable model with the accuracy of quantum mechanics, *Phys. Rev. Lett.* **120**, 143001 (2018).
- [18] L. Zhang, J. Han, H. Wang, W. A. Saidi, R. Car, and E. Weinan, End-to-end symmetry preserving inter-atomic potential energy model for finite and extended systems, in *Proceedings of the 32nd International Conference on Neural Information Processing Systems*, NIPS’18 (Curran Associates Inc., Red Hook, NY, USA, 2018) pp. 4441–4451.
- [19] M. Chen, G. Guo, and L. He, Systematically improvable optimized atomic basis sets for ab initio calculations, *J. Phys.: Condens. Matter* **22**, 445501 (2010).
- [20] P. Li, X. Liu, M. Chen, P. Lin, X. Ren, L. Lin, C. Yang, and L. He, Large-scale ab initio simulations based on systematically improvable atomic basis, *Comp. Mater. Sci.* **112**, 503 (2016).
- [21] P. Lin, X. Ren, X. Liu, and L. He, Ab initio electronic structure calculations based on numerical atomic orbitals: Basic formalisms and recent progresses, *Wiley Interdiscip. Rev.: Comput. Mol. Sci.* **14**, e1687 (2024).
- [22] M. Schlipf and F. Gygi, Optimization algorithm for the generation of ONCV pseudopotentials, *Comput. Phys. Commun.* **196**, 36 (2015).
- [23] J. P. Perdew, K. Burke, and M. Ernzerhof, Generalized gradient approximation made simple, *Phys. Rev. Lett.* **77**, 3865 (1996).
- [24] A. P. Thompson, H. M. Aktulga, R. Berger, D. S. Bolintineanu, W. M. Brown, P. S. Crozier, P. J. in ’t Veld, A. Kohlmeyer, S. G. Moore, T. D. Nguyen, R. Shan, M. J. Stevens, J. Tranchida, C. Trott, and S. J. Plimpton, LAMMPS - a flexible simulation tool for particle-based materials modeling at the atomic, meso, and continuum scales, *Comput. Phys. Commun.* **271**, 108171 (2022).
- [25] S. Grimme, J. Antony, S. Ehrlich, and H. Krieg, A consistent and accurate ab initio parametrization of density functional dispersion correction (DFT-D) for the 94 elements H-Pu,

- J. Chem. Phys.* **132**, 154104 (2010).
- [26] J. Zeng, D. Zhang, D. Lu, P. Mo, Z. Li, Y. Chen, M. Rynik, L. Huang, Z. Li, S. Shi, Y. Wang, H. Ye, P. Tuo, J. Yang, Y. Ding, Y. Li, D. Tisi, Q. Zeng, H. Bao, Y. Xia, J. Huang, K. Muraoka, Y. Wang, J. Chang, F. Yuan, S. L. Bore, C. Cai, Y. Lin, B. Wang, J. Xu, J.-X. Zhu, C. Luo, Y. Zhang, R. E. A. Goodall, W. Liang, A. K. Singh, S. Yao, J. Zhang, R. Wentzcovitch, J. Han, J. Liu, W. Jia, D. M. York, W. E. R. Car, L. Zhang, and H. Wang, DeePMD-kit v2: A software package for deep potential models, *J. Chem. Phys.* **159**, 054801 (2023).
- [27] Y. Zhang, H. Wang, W. Chen, J. Zeng, L. Zhang, H. Wang, and W. E, DP-GEN: A concurrent learning platform for the generation of reliable deep learning based potential energy models, *Comput. Phys. Commun.* **253**, 107206 (2020).
- [28] G. A. Tribello, M. Bonomi, D. Branduardi, C. Camilloni, and G. Bussi, Plumed 2: New feathers for an old bird, *Comput. Phys. Commun.* **185**, 604 (2014).
- [29] A. Laio and M. Parrinello, Escaping free-energy minima, *Proc. Natl. Acad. Sci. U.S.A.* **99**, 12562 (2002).
- [30] J. Wu, Y. Zhang, L. Zhang, and S. Liu, Deep learning of accurate force field of ferroelectric HfO_2 , *Phys. Rev. B* **103**, 024108 (2021).
- [31] J. Wu, J. Yang, L. Ma, L. Zhang, and S. Liu, Modular development of deep potential for complex solid solutions, *Phys. Rev. B* **107**, 144102 (2023).
- [32] X.-J. Song, Y.-A. Xiong, R.-J. Zhou, X.-X. Cao, Z.-Y. Jing, H.-R. Ji, Z.-X. Gu, T.-T. Sha, R.-G. Xiong, and Y.-M. You, The first demonstration of strain-controlled periodic ferroelectric domains with superior piezoelectric response in molecular materials, *Adv. Mater.* **35**, 2211584 (2023).
- [33] H. Fu and R. E. Cohen, Polarization rotation mechanism for ultrahigh electromechanical response in single-crystal piezoelectrics, *Nature* **403**, 281 (2000).
- [34] N. Hansen and C. Barlow, Plastic deformation of metals and alloys, in *Physical Metallurgy (Fifth Edition)*, edited by D. E. Laughlin and K. Hono (Elsevier, Oxford, 2014) fifth edition ed., pp. 1681–1764.
- [35] R. Guo, L. E. Cross, S.-E. Park, B. Noheda, B. Noheda, D. E. Cox, and G. Shirane, Origin of the high piezoelectric response in $\text{PbZr}_{1-x}\text{Ti}_x\text{O}_3$, *Phys. Rev. Lett.* **84**, 5423 (1999).

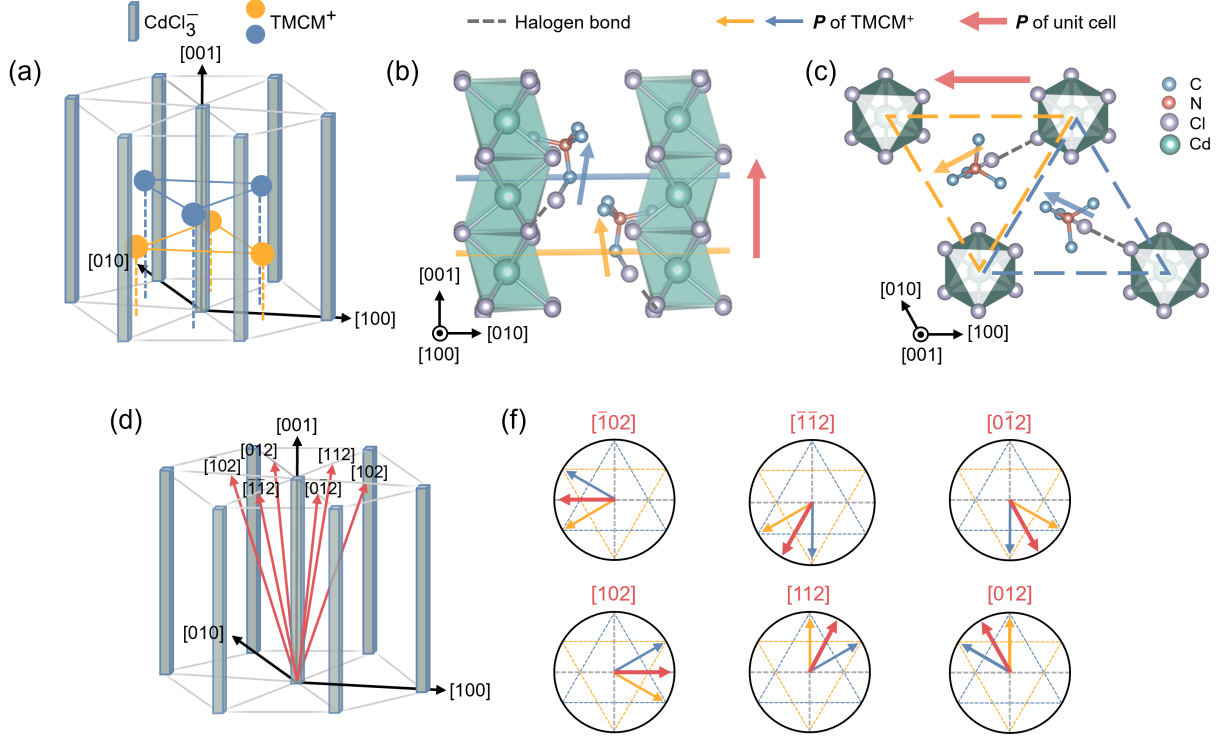


FIG. 1. **Crystal structure and polarization variants of TMCM-CdCl₃.** (a) Schematic illustration of the host-guest framework in TMCM-CdCl₃. One-dimensional inorganic CdCl₃⁻ chains form a triangular lattice, with organic TMCM⁺ cations occupying the interstitial sites to create A-B stacked triangular sub-lattices. The crystallographic axes and directions shown are defined with respect to the paraelectric hexagonal lattice. (b) Side view and (c) top view of the crystal structure in the ferroelectric phase. The dashed triangle indicates the local triple-well potential energy surface associated with the in-plane rotation of a TMCM⁺ cation, which exhibits C₃ symmetry. In this phase, molecules are anchored by highly directional CH₃-Cl \cdots Cl halogen bonds (gray dashed lines). Due to the helical arrangement of Cl atoms along the CdCl₃⁻ chain, the molecular dipoles in adjacent layers are not fully aligned. (d) Six equivalent macroscopic polarization directions in the ferroelectric phase, each with different in-plane components. (e) Schematics showing the collective in-plane orientations of molecular dipoles corresponding to the six polar variants in (d). Yellow and blue triangles represent the two dipole layers within the unit cell as shown in (b) and (c), and red arrows denote the net in-plane polarization.

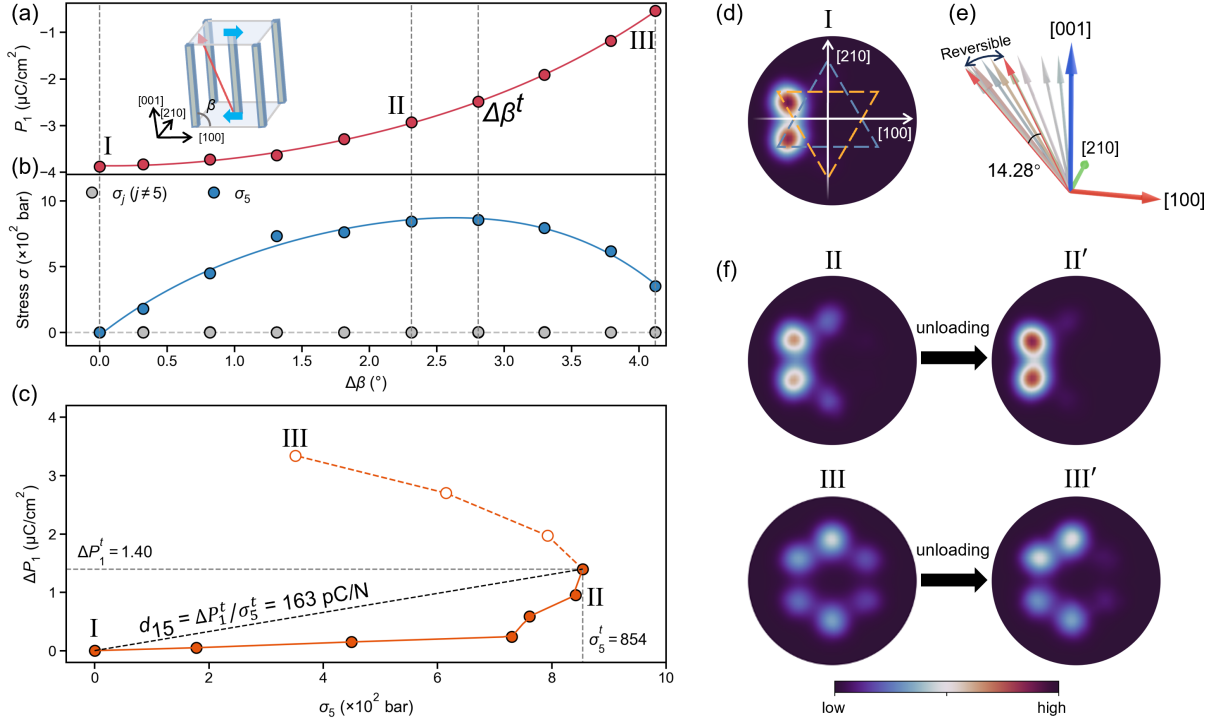


FIG. 2. Shear stress-induced reversible giant piezoelectric response via molecular dipole hopping. (a) Evolution of the polarization component along [100], P_1 , and (b) shear stress σ_5 as a function of shear strain $\Delta\beta$. The inset in (a) illustrates the initial state I, characterized by a monoclinic unit cell with in-plane polarization aligned along $[\bar{1}00]$. The shear strain is imposed by varying the lattice angle β while allowing all other lattice parameters to relax. MD simulations ensure that for a fixed $\Delta\beta$, all other stress components (σ_j , $j \neq 5$) remain negligible, as confirmed in (b). The shear stress σ_5 reaches a maximum at a critical strain $\Delta\beta^t$. (c) Polarization change ΔP_1 as a function of σ_5 , derived from (a) and (b). (d) In-plane dipole orientation density plot for TMCM⁺ cations in the initial state I, following the schematic in Fig. 1. (e) Reversible region for the rotation of the macroscopic polarization. $\Delta\beta_t$ corresponds to a small rotational angle of 14.28° . (f) Dipole orientation density plots for strained states II and III, and their corresponding relaxed configurations after unloading (II' and III'). The transition between states I and II is reversible, while the transition from I to III is irreversible as III' is different from I.

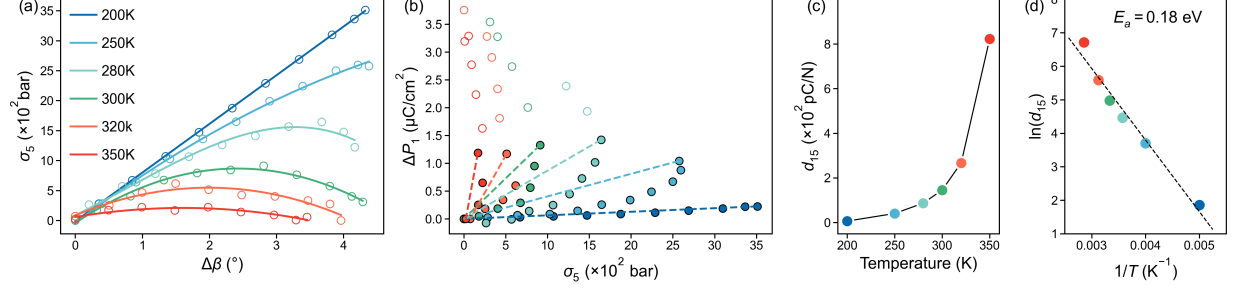


FIG. 3. **Temperature-dependent piezoelectric response of TMCM- CdCl_3 .** (a) Shear stress-strain curves obtained from MD simulations at temperatures ranging from 200 K to 350 K. Solid lines represent polynomial fits to the simulation data. (b) Corresponding polarization change ΔP_1 as a function of applied shear stress σ_5 at each temperature. The piezoelectric coefficient d_{15} is extracted from the reversible response region, indicated by solid markers. (c) Temperature dependence of d_{15} . (d) Arrhenius plot of $\ln d_{15}$ versus $1/T$, with the dashed line indicating a linear fit. The slope yields an activation energy of $E_a = 0.18$ eV.

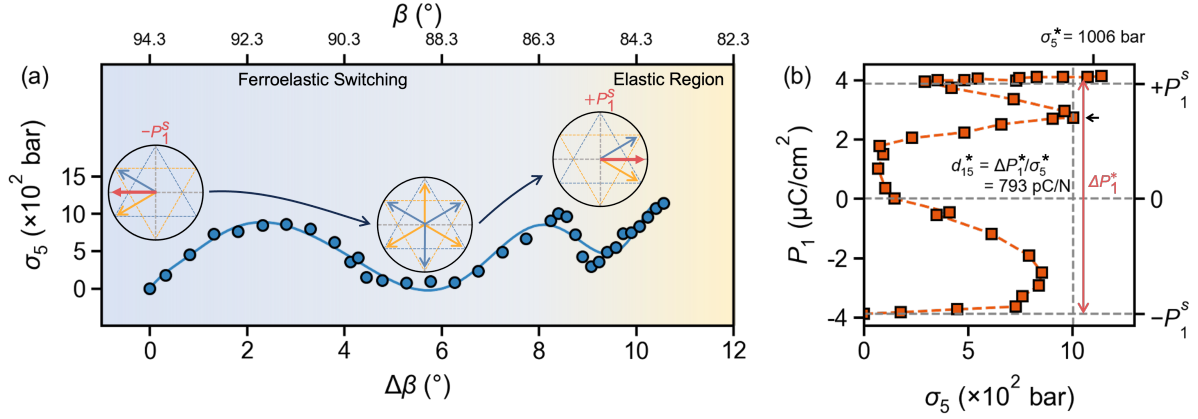


FIG. 4. **Ferroelastic switching driven by large shear stress.** (a) Shear stress–strain curve corresponding to a full reversal of in-plane polarization ($-P_1^s \rightarrow +P_1^s$) driven by shear stress σ_5 . Insets illustrate the in-plane orientations of molecular dipoles during the switching process. The stress exhibits a characteristic increase followed by a decrease, reminiscent of the plastic deformation behavior observed in metals. An intermediate state near $\beta \approx 90^\circ$ shows a nearly isotropic distribution of in-plane dipoles. Upon completing the switching, the system enters an elastic regime where stress increases linearly with strain. (b) Hysteresis loop showing the relationship between shear stress σ_5 and polarization P_1 during the switching process in (a). The maximum stress σ_5^* defines the threshold required to complete the ferroelastic switching. The corresponding maximum (irreversible) piezoelectric response is estimated as $d_{15}^* = \Delta P_1^s / \sigma_5^*$.